University of North Carolina Asheville
Journal of Undergraduate Research
Asheville, North Carolina
Spring 2024

Event-based Verification of IMERG V06 Precipitation Estimates Over Complex Terrain in the Southern Appalachian Mountains

Dylan Major
Atmospheric Sciences, Computer Science, and Mathematics
The University of North Carolina Asheville
One University Heights
Asheville, North Carolina 28804 USA

Faculty Mentor(s):

Dr. Douglas Miller
Dr. Christopher Godfrey

Abstract

In addition to helping climatological studies, accurate precipitation maps can help determine the degree of drought and flooding. The Integrated Multi-satellitE Retrievals for the Global (IMERG) Precipitation Mission utilizes quantitative precipitation estimates (QPEs) to create worldwide precipitation maps. IMERG grid cells are bounded by 0.1° latitude by 0.1° longitude sides, which in the mid latitudes is close to 100 km2. Ground-based rainfall observations can help to verify the calibration of the satellites. However, even with proper calibration, precipitation can vary greatly over a 100 km2 area, especially if there is a substantial variation of terrain elevation and/or the atmospheric features generating the precipitation are convective in nature. This project compares the precipitation measurements of the Duke Great Smoky Mountains Rain Gauge Network (GSMRGN) between individual rain gauges of the network and with IMERG QPEs. An analysis is done on the daily scale from July 2009 through October 2021 looking at correlation, bias, and several other statistical measures. With these, less agreement is found between IMERG grid cells and collocated GSMRGN gauges

with events of finer spatial and temporal scale and in the warm season, defined as the months of June, July, and August. Additionally, direction of propagation of rainfall events is identified through the GSMRGN records and correlation between rainfall measurements of gauges is shown to vary based on direction.

Introduction

Segregating precipitation by event type provides a robust analysis and physically-based error diagnostic study when comparing in-situ observations with gridded remotely sensed estimates. In this sense we are able to provide a better verification of satellite-based precipitation estimates.

Maintaining a spatially dense and long-term ground observational network over complex terrain is challenging due to the remote accessibility and sparse inhabitation (e.g., Barstad and Smith 2005). Moreover, orographic precipitation is highly heterogeneous and greatly depends on topographic influence (Houze 2012; Barros 2013). To bridge the gap in the availability of observations over mountain regions and ridges a high-quality, spatially dense rain gauge network was established in 2007 in western North Carolina, the Duke Great Smoky Mountain Rain Gauge Network (Duke GSMRGN). This rain gauge network includes 32 tipping bucket rain gauges that are located at the mid to high elevations on exposed ridges of the Southern Appalachian Mountains to provide high spatial resolution precipitation observations over the Pigeon River Basin (PRB) (e.g., Prat and Barros, 2010a; Prat and Barros, 2010b; Barros et al. 2014; Miller et al. 2018).

This ability to observe and accurately quantify precipitation in the PRB has societal impacts. Heavy rainfall in the PRB would trigger extensive flooding and landslides affecting the lives and livelihoods of the public. For example, in August 2021, significant rainfall from the remnants of Tropical Storm Fred caused severe flooding in the PRB especially around Canton, NC leading to multiple deaths and damages around $18 million (Cardwell 2022). Other examples include the occurrence of two heavy rainfall events in 2020 over the region that triggered landslides and flash flooding (Miller et al 2021a; Miller et al 2021b). High-quality observations of mountainous rainfall processes can lead to better understanding and forecasting of related hazards such as flooding, debris flow, and landslides.

However, other mountainous regions do not have a rain gauge network like the Duke GSMRGN. Additionally, there are precipitation effects that point measurements such as gauges can miss.

While ground observations provide the direct measurements of precipitation, maintaining a consistent, long-term, spatially dense network is a challenging task. For remote regions lacking continuous ground observations, Satellite precipitation products, such as the Integrated Multi-satellitE Retrievals for the Global Precipitation Mission (IMERG; Huffman et al. 2020) provide comprehensive and gridded quantitative estimates of precipitation thereby filling the gap in in-situ measurements. However, satellite precipitation products provide indirect estimates of precipitation and typically prone to detection and estimation errors due to sensor and retrieval artifacts (Hirpa et al. 2010; Duan et al. 2014; Prat and Nelson, 2015; Derin et al. 2019; Gan et al. 2021; Derin and Kirstetter 2022). The rain gauge network in a mountainous region such as the Duke GSMRGN can serve as an independent reference for validation of satellite QPEs, thereby identifying the sub-grid scale effects of topography to aid the interpretation of satellite QPEs.

The Duke GSMRGN is especially useful for validation of IMERG. It contains 32 gauges installed over 3 parallel mountain ridges ranging from about 1000 – 2000 m in elevation. Most other rain gauges in mountainous regions tend to be at lower elevations than the surrounding region, and as a result, they can miss orographic enhancement of rainfall. The gauges of the Duke GSMRGN tend to be at high elevations compared to the region. Furthermore, other high quality rain gauges like GHCN are included in calibrations of satellite precipitation products like IMERG (Huffman et al. 2020). The Duke GSMRGN is not, so it can be used as independent evaluation.

One of the systematic errors in satellite-based sensors can be due to the presence of multi-layered clouds. When high clouds (seeder clouds) precipitates over low-level cap clouds (feeder clouds), there will be an increase in drop coalescence efficiency which leads to increased surface precipitation (Hill et al. 1981; Purdy et al. 2005; Wilson and Barros 2014; Duan and Barros, 2017; Arulraj and Barros, 2019). Seeder-feeder precipitation events make up a large part of mountain weather systems contributing to approximately fifty percent of precipitation recorded by the Duke GSMRGN from the period of 2007–2013 (Houze 2012; Wilson and Barros 2014). Previous studies observe the presence of high detection and estimation bias in satellite derived quantitative precipitation estimates (QPEs) that are tied to the diurnal and seasonal cycles of the seeder-feeder precipitation systems (Prat and Barros 2010b; Duan et al 2014; Arulraj and Barros, 2019). These underestimations in satellite-based QPEs can lead to timing errors in flash flood and landslide forecasting (Tao and Barros, 2013; Maggioni and Massari, 2018; Hinge et al 2022).

Another challenge in interrupting satellite derived QPEs is that the data they provide are coarse. For instance, the spatial resolution of IMERG is 0.1° (Huffman et al. 2020). This footprint is over 80 km2 at the latitude of the PRB. Precipitation over an 80 km2 area can range greatly, especially in the mountains. Using the Duke GSMRGN data record, Prat and Barros (2010a) found that daily average precipitation can vary by

300% over a distance less than 8 km. Seasonal effects can exacerbate the challenges presented by lack of resolution. In the warm season, June, July, and August, convective precipitation is common in this region. If a particular convective event is not too fine in resolution for the satellite QPE to register, the precipitation from it still has to be smoothed out over the entire 80 km2 QPE. Localized effects that could result in flash flooding are missed.

The retrieval algorithm and the assumptions involved could also lead to errors in satellite based QPEs. Satellite QPE algorithms are typically applied globally and therefore are developed for assumptions that hold for a wide range of circumstances. As a result, misinterpretation and misidentification of mountain weather systems can occur (Prat and Barros 2010b; Duan et al 2014; Arulraj and Barros, 2019). Specifically, a classical, albeit oversimplified, understanding of mountain weather is that higher elevations get more precipitation due to adiabatic cooling of rising air. Prat and Barros (2010b) found that ridges received twice the precipitation than the valleys did during September through November of 2008 in the PRB. If this understanding applies to other seasons as well, precipitation measurements at higher elevations should exhibit larger bias and larger variance. Satellite precipitation estimation involves complex processing steps that result in an areal average of precipitation that is different than the corresponding point observation. As an example, the satellite QPEs factor the entire area (e.g., valleys and peaks) when generating the precipitation observation, possibly resulting in a lesser variable observation. This could cause underestimation of satellite based QPEs with respect to the ground observations in mountain regions.
Even though the rain gauges best capture the precipitation, there are some errors associated with gauge observations as well. Rain gauge undercatch is a documented error related to in-situ observations (e.g., Duchon et al. 2014). This undercatch is manifested in the reported observations as a random error which can result in a larger bias when used for validation studies (WMO 2008). Other random errors exist in in-situ observations such as sitting, exposure, evaporation, force of falling water, and bearing friction (WMO 2008).

We outline a novel method that is based on event-based analysis for comparing in-site observations and satellite-based observations. Specifically, more than a decade of precipitation observations from Duke GSMRGN are compared with satellite based QPEs such as the IMERG. The ability of IMERG to detect and estimate precipitation is analyzed and the errors are documented with respect to the season and direction of the events.

Section 2, Data and Methods, will provide details on the Duke GSMRGN and IMERG and methods used to compare the two including how events and directionality are determined and defined. Data and Methods finishes with a brief justification for the separation by seasonality. Section 3, Results, compares collocated IMERG QPEs and Duke GSMRGN gauges using standard detection metrics and proceeds to focus on

regional differences when looking seasonally at the detection metrics. After it looks at biases for all data and seasonally. Next it looks at event direction. It does this with correlation versus distance between Duke GSMRGN gauge measurements and biases. Section 4, Discussion, looks into possible reasons for some of the biases found. We end in section 5 with conclusions.

Data and Methods

Duke Great Smoky Mountain Rain Gauge Network

The Duke GSMRGN contains 32 tipping bucket rain gauges installed over 3 parallel sets of mountain ridges ranging from about 1000 – 2000 m in elevation (Barros et al. 2014; Miller 2022). Accordingly, gauges are separated into three groups designated by the first digit of the gauge number. Gauges starting with a '3' are located on the northwest ridges and are gauge model TB1 with a sensitivity of 1 mm/tip, gauges starting with '1' are located on the central ridges and are gauge model TB3/0.1 with a sensitivity of 0.1mm/tip, and gauges starting with '0' are located on the southeast ridges and are gauge model TB3 with a sensitivity of 0.2 mm/tip (Duke 2022). Field maintenance on each gauge is performed every 2 to 3 months and quality control metrics are evaluated as described in Miller 2022. Data with quality control flags that influence precipitation quantity or timing were removed. This includes flags that indicate temporary debris located in gauge, a clogged gauge, electrical contact problems, a missing period of data, and the date stamp to be unreliable. The first gauges in the network were deployed in 2007. All gauges were deployed by July 1st 2009, and consequently, the period of record used was July 1st 2009 through October 17th 2021. Table A1 in Appendix A shows the latitude, longitude, and elevation for each of the named gauges in the network. More information on the gauges and maintenance can be found in Miller 2022.

Integrated Multi-satellitE Retrievals for the Global Precipitation Mission (IMERG)

The IMERG Precipitation Mission utilizes InfraRed (IR) and Passive Microwave (PMW) QPE products to create global QPEs at 0.1° spatial and half-hourly temporal

resolution (Huffman et al. 2020). Version-06 dataset was used for this study (Huffman et al. 2020).

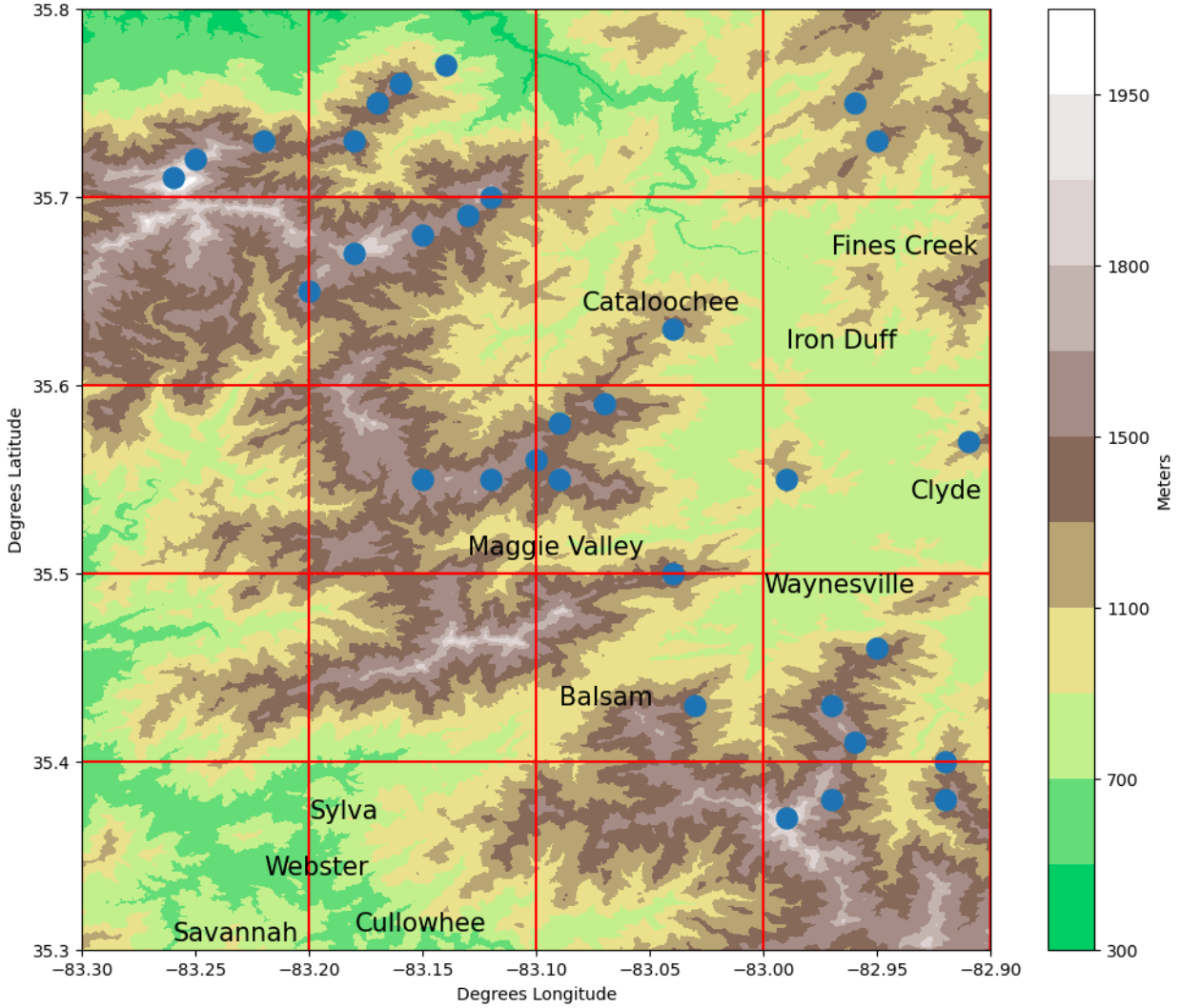

Figure 1. Elevation map of the Pigeon River Basin (PRB). The points indicate the locations of GSMRGN gauges and the red cross hairs separate IMERG QPEs. The black points show the gauges in the central ridges while blue points mark the gauges in the outer ridges. Elevation data source: USGS.

The study region, the PRB, is shown in Figure 1. The area in Figure 1 has a peak elevation of 2019 meters and an average elevation of 1063 meters (U.S. Geological Survey 2022). The 32 gauges that make up the GSMRGN provide an opportunity to study subgrid scale topographic effects that contribute to interpreting IMERG QPEs in the PRB and similar regions.

IMERG Validation

Standard detection metrics are used to evaluate the agreement between IMERG and the Duke GSMRGN: hits, misses, false alarms, and correct nos. Hits are defined as the total number of days when a gauge and corresponding IMERG QPE both recorded at least 1 mm of precipitation. Misses describe cases where the IMERG QPE records less than 1mm when one of the collocated rain gauges exceeds that threshold. False alarms identify scenarios when the IMERG QPE records 1 mm or more of rain, but none of the collocated rain gauges exceed that threshold. Correct nos are days where both products report less than 1mm of rain.

Event Definition and Classification

The study considers precipitation events during the 2009-2021 time period by performing detection and evaluation analyses. A unique event was defined to start at the beginning of the hour when at least one Duke GSMRGN gauge tipped while all gauges recorded no precipitation the previous hour. That event was defined to end at the beginning of the next hour when there was no precipitation recorded at any gauge during that given hour. For each event, linear regressions of the time each gauge first recorded precipitation and the latitude/longitude of the gauges were used to determine the direction of propagation of an event. Events were considered directional if

$$r > e^{-1+\frac{\pi}{n}}$$

where r is the Spearman rank correlation coefficient of the regression and n is the number of gauges recording precipitation during an event. Rank correlation was used as opposed to Pearson correlation because it is independent from the speed the storm is moving at, which may not be constant. One plus π over n was chosen because it requires at least four gauges to record precipitation and approaches e^{-1} for decorrelation with an infinite number of gauges. Linear regressions of three points and times would likely predict all three in the right order regardless of actual directionality. This also helps to separate out isolated events that may not have encountered all of the topography larger directional events would.

This method of determining direction captures the initial local direction of propagation, which may or may not match the synoptic direction. The local direction is a better indicator of the specific topography the precipitation event traversed and experienced orographic influence from in the PRB than the synoptic direction. This is because this method is derived from an estimate of the path the precipitation event took through the PRB. However, initial direction does not always reflect the direction of the storm during the whole duration of the event.

Seasonality

Winter was defined as December, January, and February (DJF); spring as March, April, and May (MAM); summer as June, July, and August (JJA); and fall as September, October, and November (SON).

Summer versus non-summer analyses were separated due to the convective nature of much of the precipitation during these months. Figure 2 shows the lower correlation of the summer analysis versus the non-summer analysis.

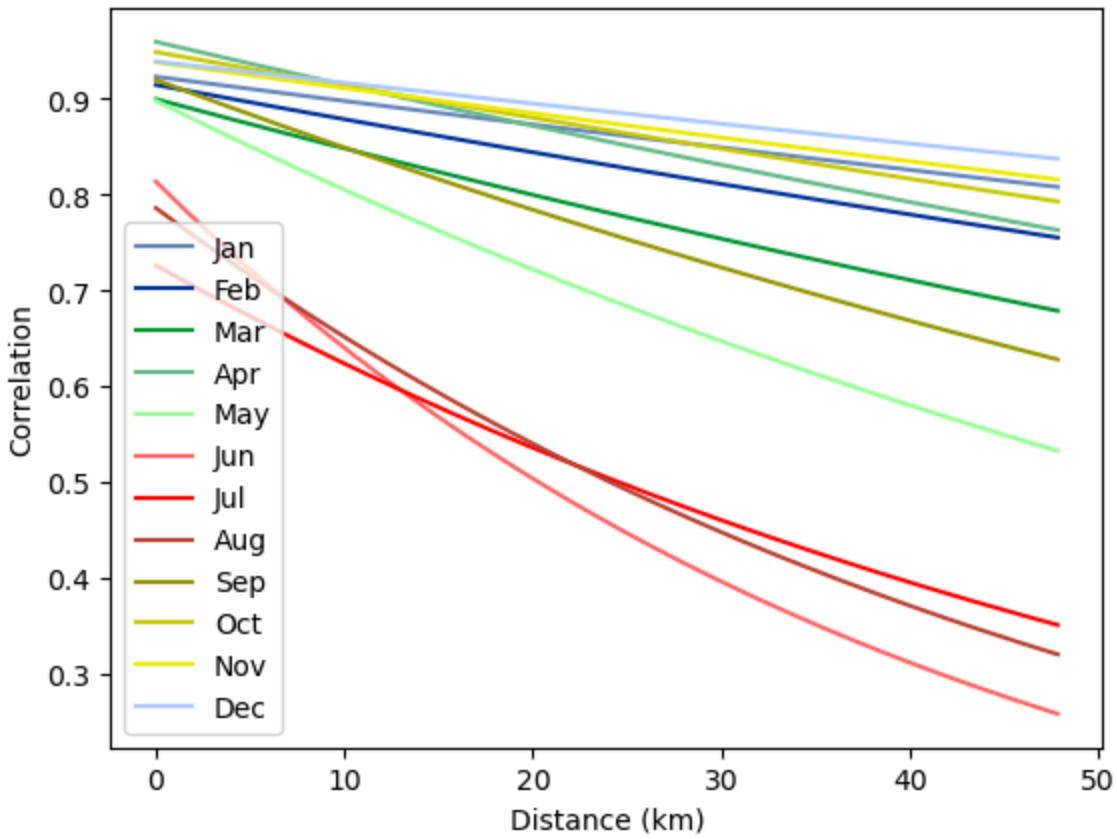

Figure 2. Exponential regressions of the Pearson correlation coefficient of daily gauge precipitation measurements and the distance between the gauges.

Results

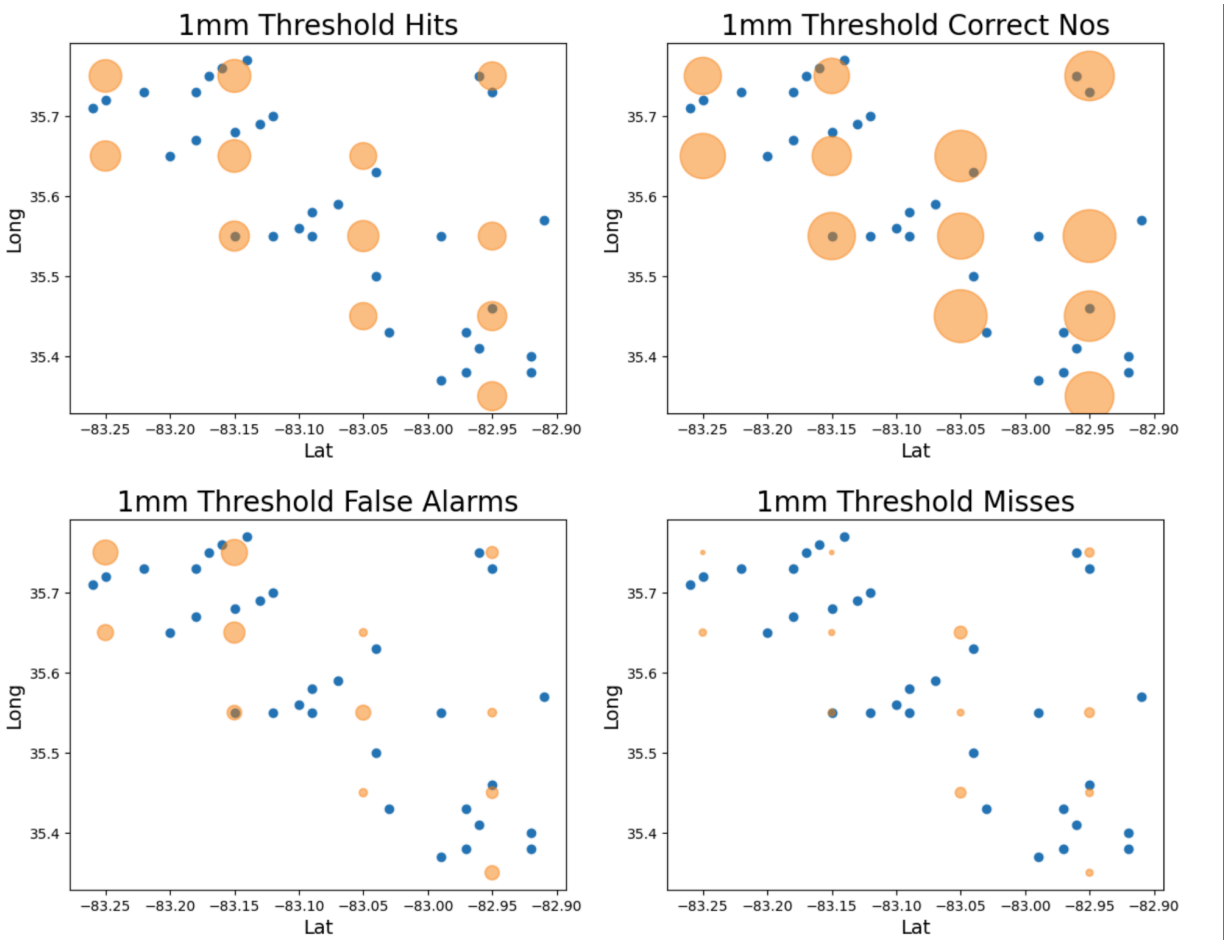

Figure 3. Hits, misses, false alarms, and correct nos with a 1mm daily threshold. The blue circles are the location of the gauges. The orange circles' radii represent the proportion of days for each IMERG QPE matching a given detection metric.

Overall, the IMERG QPEs perform well at detecting precipitation events. Their records match the gauges on what days it did and did not precipitate for the majority of days (Figure 3). There is little spatial correlation in the hits, but there are more false alarms and fewer correct nos in the northwest part of the PRB region (Figure 3). This may be in part due to snow, which the northwest receives more of. The gauges are not heated, so they do not measure snow until it melts. If it is sufficiently cold enough for less than 1mm of liquid equivalent of snow to melt on a snow day, this would lead to the erroneous recording of a false alarm. However, snow events are relatively rare in the Southern Appalachians, and if snow was responsible, one would expect an erroneous increase in misses when the snow melts over the next few successive days. This is not observed in the misses (Figure 3). That being said, IMERG uses passive MW observations. Consequently, snow can sometimes cause a false alarm or an erroneous hit instead of a miss, so the lack of misses does not completely rule out snow. A seasonal look at the false alarms could help to further assess the effect of snow.

Season	Proportion of days that are false alarms NW gauges (NW)	Proportion of days that are false alarms other gauges (OG)	NW / OG
Winter	0.180	0.357	1.987
Spring	0.111	0.200	1.801
Summer	0.085	0.153	1.797
Fall	0.091	0.188	2.069

Table 1. Daily false alarm rates by season comparing the Northwesternmost 4 QPEs to the other QPEs. Values are proportions of days.

Snow cannot account for the higher rate of false alarms in the northwest. There are roughly twice as many false alarms in the NW gauges as compared to the other gauges in all seasons (Table 1). However, there is a higher rate of false alarms in the winter across all gauges. Snow can contribute to this.

Despite the higher rate of false alarms, the northwestern IMERG QPEs have a low bias compared to the collocated gauges (Figure 4). This is true for most gauges, both around 2000 m and 1500 m, in those QPEs (Figure 4). They are reporting more days of precipitation but less total precipitation. These are the QPEs with fewer or no mountains to their northwest. Looking seasonally, the low bias in the IMERG QPEs occurs in spring, fall, and especially summer (Figure 5). Convective precipitation may contribute to the higher magnitude of bias in summer months as it is small scale and has to get smoothed out over the whole IMERG QPE, so it may be missed or underreported.

Both the differences between gauges and collocated IMERG QPEs related to false alarms and average precipitation have been in the northwest of the region. This area is the most exposed to NW flow and suggests that there may be differences between gauge and QPE measurements based on the direction of propagation of the storm.

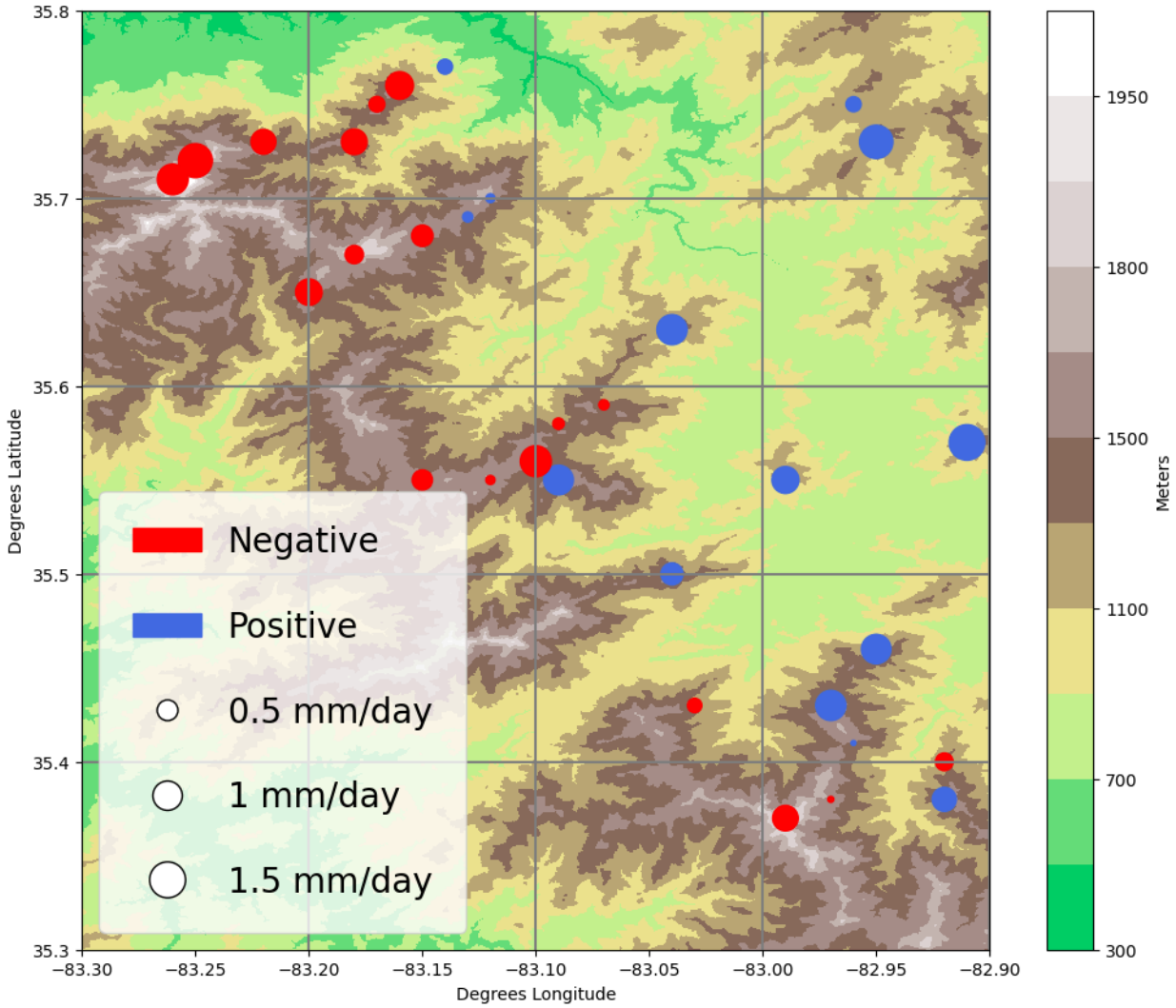

Figure 4. Daily precipitation IMERG bias by gauge (IMERG - gauge). The gray crosshairs separate individual IMERG QPEs grid boxes. The points are at the location of the gauges and the size of their radius represents the IMERG QPE bias compared to the gauge measurement. Red is a negative bias. Blue is a positive bias. The background color is the elevation in meters from USGS data.

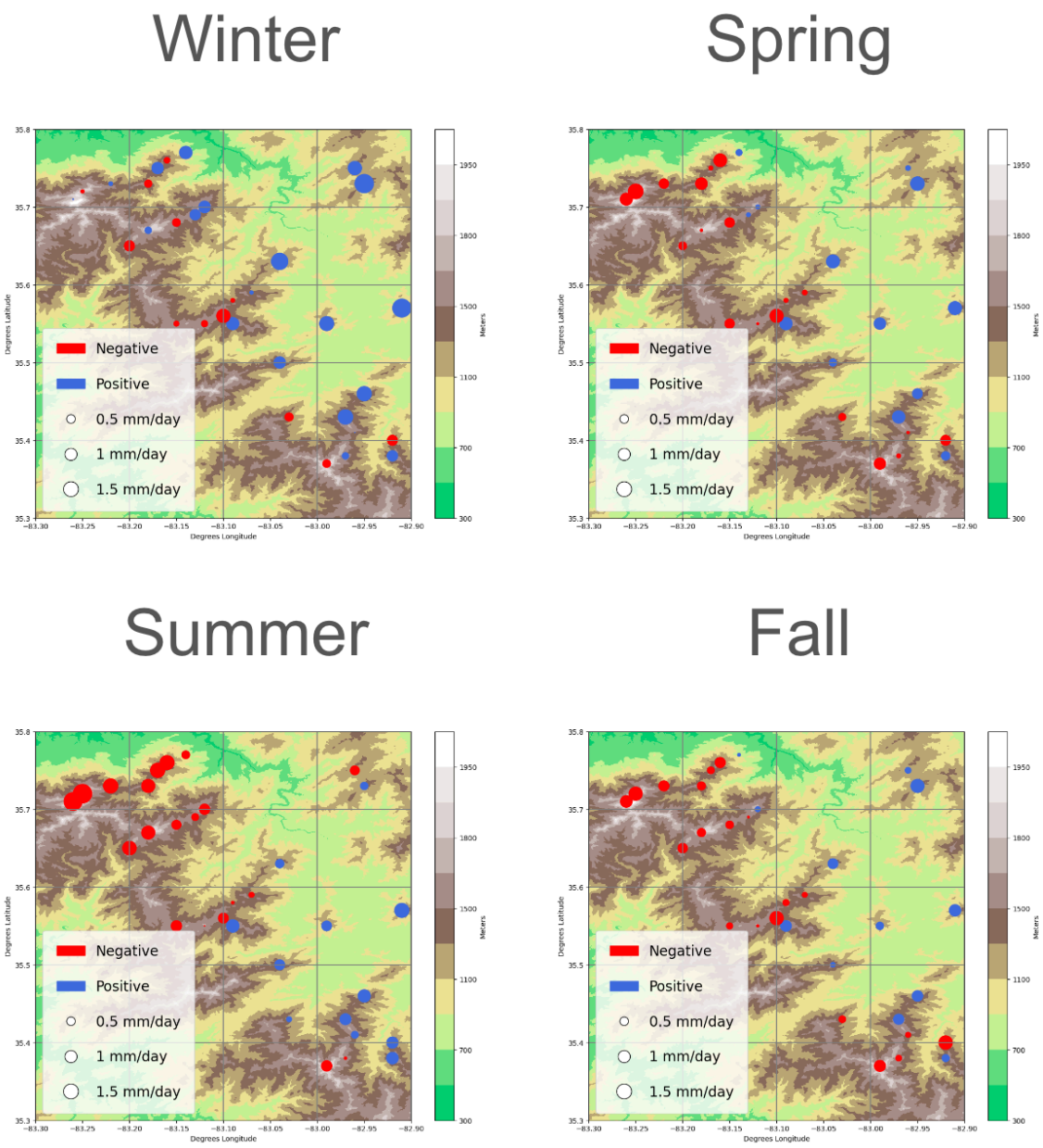

Figure 5. Same as Figure 4, separated by season.

Considering directionality, NE events were included for completeness as they are rare and there are not many synoptic patterns that bring in storms from the NE. SE events have higher correlation compared to all events year-round and in the summertime for all distances (Figure 6). The same is true for year-round SW events as compared to all events, especially with greater separation between gauges (Figure 6). For summertime, SW events also have higher correlation compared to summertime events except at very close distances where the regression values are similar enough that the confidence intervals overlap (Figure 6). NW events were an exception. NW

events had higher correlation at short distances, but for the year-round category, drop below all events at around 10 km (Figure 6). This sharp drop in correlation poses a challenge for QPEs with 0.1° resolution, which is about 10 km at this latitude. Directionality, especially if it is a NW event, is important when interpreting IMERG QPEs.

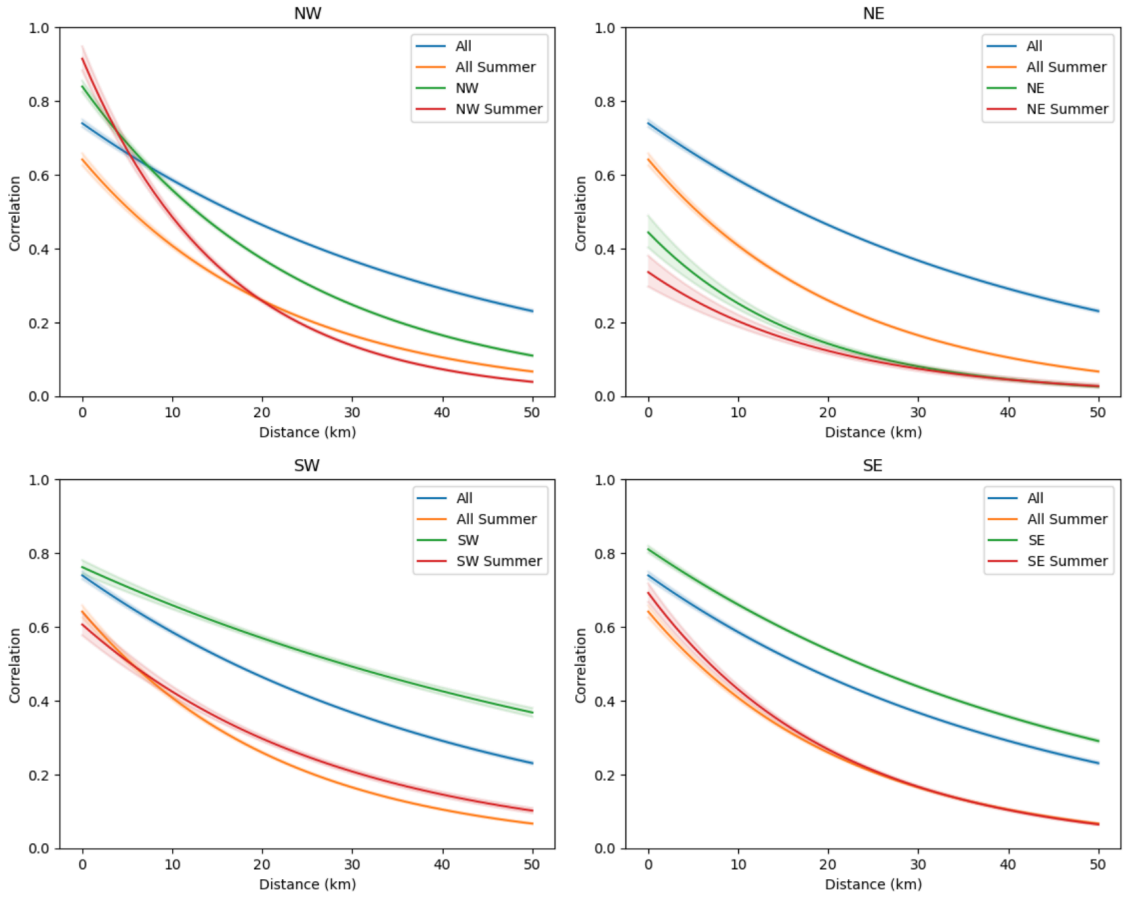

Figure 6. Exponential regressions with confidence intervals of hourly based gauge correlation by distance between gauges for each direction compared to all summer and all events.

In addition to having a sharp drop in correlation between gauge measurements during NW events, IMERG QPEs have a strong negative bias in the northwestern part of the region and slight positive bias elsewhere (Figure 7). Interestingly, a similar phenomenon is seen in SE events though it is less uniform and there are negative biases in the southeastern part of the region (Figure 7). This is not seen in SW events where IMERG tends to have a positive bias, especially in the central part of the PRB (Figure 7). These directional differences further reiterate the need to consider directionality of an event when interpreting IMERG QPEs.

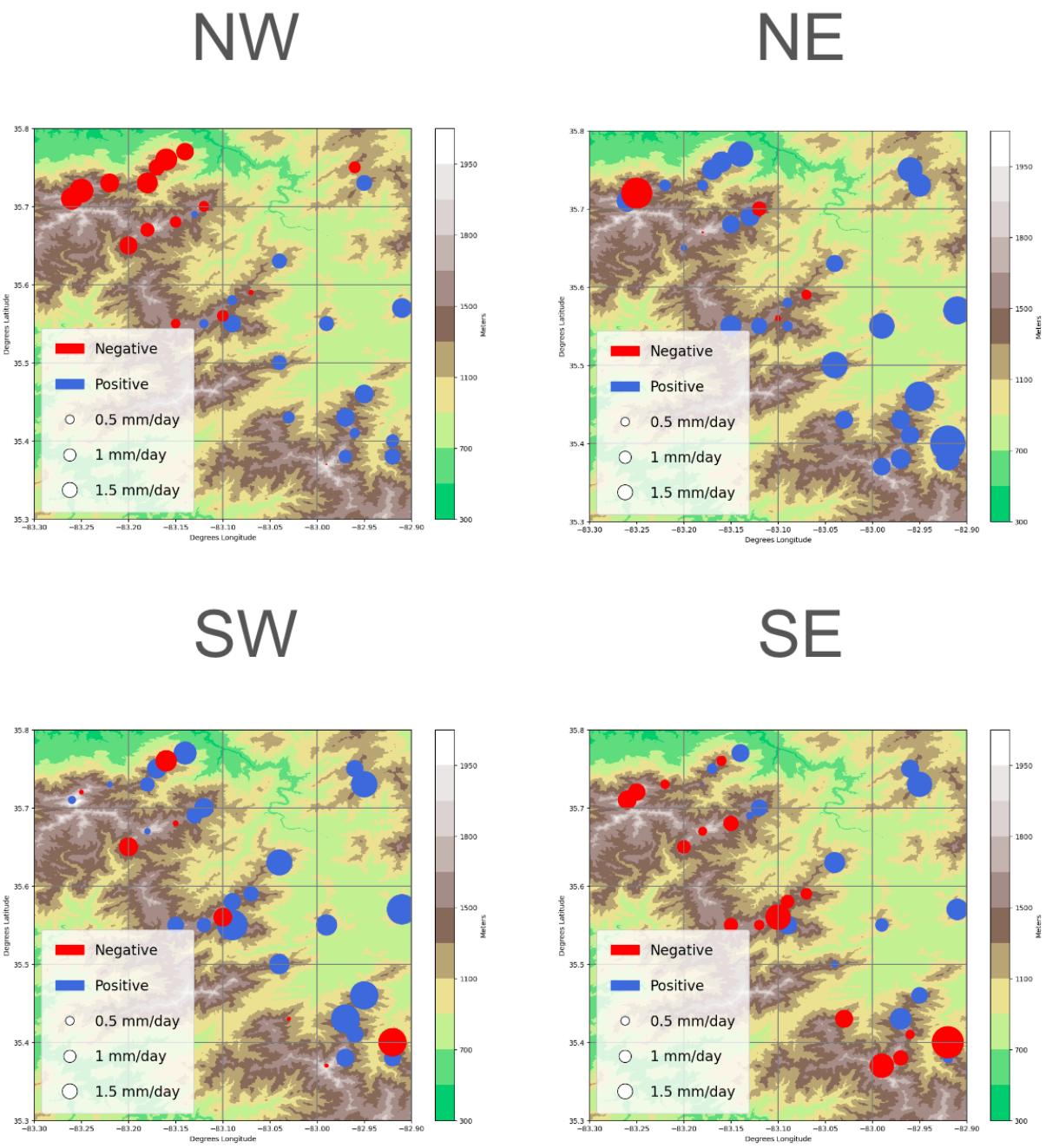

Figure 7. Same as Figure 4, separated by direction of event propagation.

Discussion

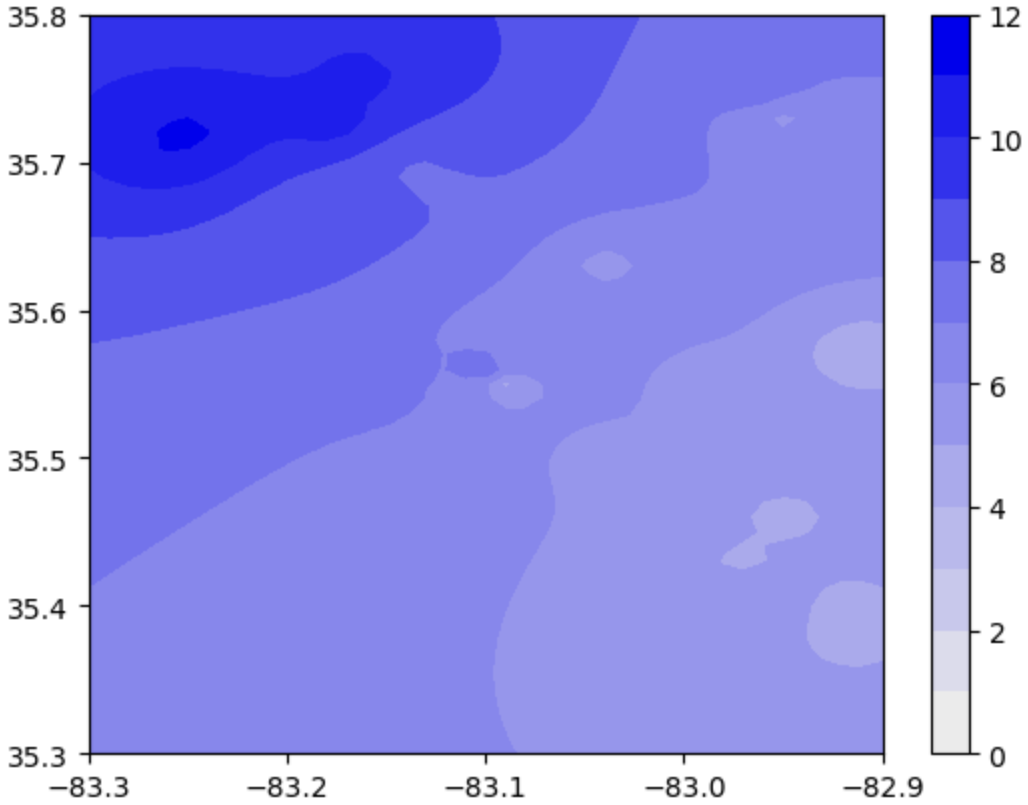

Figure 8. Mean precipitation from NW events in mm produced from inverse distance squared weighting of GSMRGN gauge measurements. Latitude and longitude are on the y- and x-axes respectively.

One possible explanation for the observed drop in correlation with distance and the differences in the gauges and QPEs in the NW is that during northwest flow events, moisture does not always make it past the first few ridgelines. With a small, uncertain amount of moisture making it past the first few ridges, precipitation amounts will not have a strong linear correlation between upstream (NW) and downstream (SE). This conceptualization is supported by Figures 8 and 9. Figure 8 shows that the NW receives over double the precipitation that the SE does during NW events. This suggests that precipitation does not always make it past the first few ridge lines. Furthermore, Figure 9 shows that there is much more precipitable water during NW than SE events, the other predominant direction of storm propagation in the PRB. This connects a lack of moisture as a possible reason for the uncertainty of precipitation downstream in NW events. With subgrid scale topography causing this drop off, it cannot be captured by 0.1° resolution.

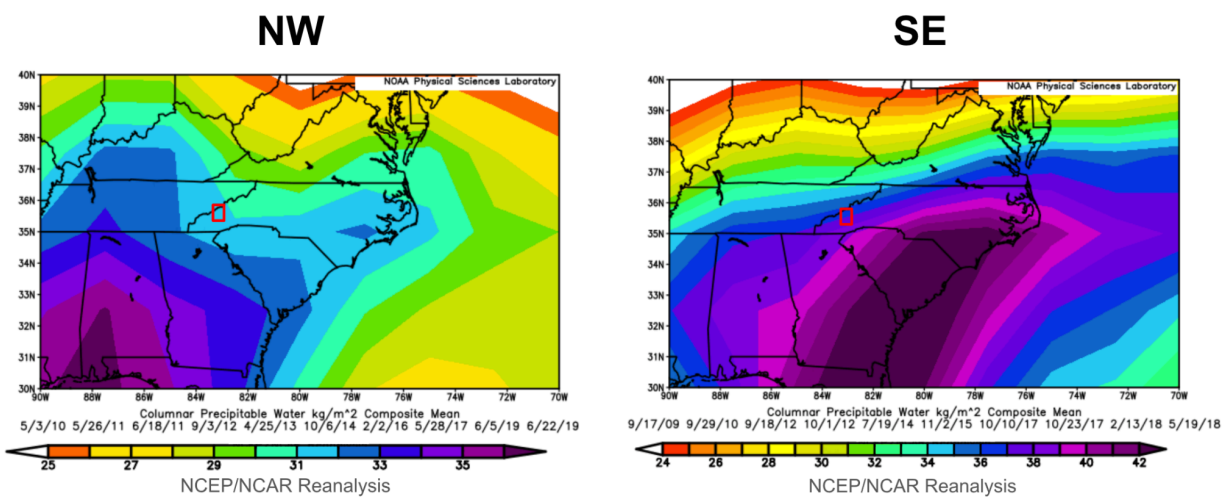

Figure 9. Composite 10-day mean columnar precipitable water for Northwest and Southeast events. Of events with all operational gauges reporting rain and at least 25 operational gauges, the 10 with the highest rank correlation for their direction of propagation were chosen. The first day of the event was chosen unless more hours of the event occurred on the second day. List of the exact dates is below each graph. NCEP-NCAR Reanalysis 1 Data provided by the NOAA PSL, Boulder, Colorado, USA, from their website at https://psl.noaa.gov.

IMERG and the Duke GSMRGN have a reasonable level of agreement. There are some differences in the NW where the area is exposed to NW flow events. Looking into this, directionality was shown to have an influence on how fast correlation between precipitation measurements drops with distance between two points, especially for NW events. Furthermore, biases between events with different directionality were shown to be different. Consequently, directionality is important for interpreting IMERG QPEs in mountainous regions. This is particularly true for subgrid scale phenomena and high resolution QPEs may be useful in the PRB.

Acknowledgements

Thank you to the “Mountain Rangers” who provide regular maintenance on the Duke GSMRGN and Duke University for funding the network, Dr. Elaine Godfrey for providing helpful edits and comments, and Dr. Douglas Miller and Dr. Christopher Godfrey for being faculty mentors.

References

Arulraj, M., and Barros, A. P., 2019: Improving quantitative precipitation estimates in mountainous regions by modeling low-level seeder-feeder interactions constrained by Global Precipitation Measurement Dual-frequency Precipitation Radar measurements. *Remote Sensing of Environment*, **231**, 111213, https://doi.org/10.1016/j.rse.2019.111213.

Barros, A. P., 2013: Orographic precipitation, freshwater resources, and climate vulnerabilities in mountainous regions. *Climate Vulnerability*, 5, 57–78, https://doi.org/10.1016/B978-0-12-384703-4.00504-9.

Barros, A. P., W. Petersen, M. Schwaller, R. Cifelli, K. Mahoney, C. Peters-Liddard, D. Starr, 2014: NASA GPM-Ground Validation: Integrated Precipitation and Hydrology Experiment 2014. *Science Plan. Tech. Rep*, Duke University, Durham, U. S. A. Barstad, I., and R. B. Smith, 2005: Evaluation of an orographic precipitation model. *J. Hydrometeor.*, **6**, 85–99, https://doi.org/10.1175/JHM-404.1.

Cardwell, J., 2022: Disruption to EMS service during flood scenarios in Western North Carolina. *Journal of Rural Social Sciences*, **37**, https://egrove.olemiss.edu/jrss/vol37/iss3/6.

Derin, Y., and P.E. Kirstetter, 2022: Evaluation of IMERG over CONUS complex terrain using environmental variables. Geophysical Research Letters 49, no. 19: e2022GL100186. Derin, Y., et al. “Evaluation of GPM-era global satellite precipitation products over multiple complex terrain regions.” Remote Sensing 11.24 (2019): 2936.

Duan, Y., A. M. Wilson, and A. P. Barros, 2015: Scoping a field experiment: Error diagnostics of TRMM Precipitation Radar estimates in complex terrain as a basis for IPHEx2014. *Hydrol. Earth Syst. Sci.*, **19**, 1501–1520, https://doi.org/10.5194/hess-19-1501-2015.

Duan, Y., and A.P. Barros, 2017: Understanding how low-level clouds and fog modify the diurnal cycle of orographic precipitation using in situ and satellite observations. *Remote Sens.*, **9(9)**, 920, https://10.3390/rs9090920.

Duchon C., C. Fiebrich, and D. Grimsley, 2014: Using high-speed photography to study undercatch in tipping-bucket rain gauges. *J. Atmos. Oceanic Technol.*, **31**, 1330–1336, https://doi.org/10.1175/JTECH-D-13-00169.1.

Duke: Integrated Precipitation & Hydrology Experiment (IPHEX). Duke Great Smoky Mountains Rain Gauge Network, NC, Duke University Civil and Environmental Engineering, Accessed: June 2022. https://iphex.pratt.duke.edu/long-termRGDuke.

Epstein, E., and A. Barnston, 1990: A precipitation climatology of 5-day periods. *J. Climate*, **3**, 218–236.

Gan, F., Y. Gao, and L. Xiao. 2021: Comprehensive validation of the latest IMERG V06 precipitation estimates over a basin coupled with coastal locations, tropical climate and hill-karst combined landform. *Atmospheric Research*, **249**, 105293, https://doi.org/10.1016/j.atmosres.2020.105293.

Hill, F., K.A. Browning, M.J. Bader, 1981: Radar and rain gauge observations of orographic rain over south Wales, *Q. J. R. Meteorol. Soc.*, **107**, 643-670, https://doi.org/10.1002/qj.49710745312.

Hirpa, F. A., M. Gebremichael, and T. Hopson (2010): Evaluation of high-resolution satellite precipitation products over very complex terrain in Ethiopia. *Journal of Applied Meteorology and Climatology*, **49**, 1044-1051, http://dx.doi.org/10.1175/2009JAMC2298.1.

Houze, R. A., 2012: Orographic effects of precipitating clouds, *Rev. Geophys.*, **50**, Article RG1001, https://10.1029/2011RG000365.

Huffman, G. J., D. T. Bolvin, D. Braithwaite, K. Hsu, R. Joyce, C. Kidd, E. J. Nelkin, S. Sorooshian, J. Tan, P. Xie, 2020: NASA Global Precipitation Measurement (GPM) Integrated Multi-satellitE Retrievals for GPM (IMERG). Algorithm Theoretical Basis Document (ATBD) Version 06, 39 pp., https://gpm.nasa.gov/sites/default/files/2020-05/IMERG_ATBD_V06.3.pdf

Huffman, G. J., E. F. Stocker, D. T. Bolvin, E. J. Nelkin, J. Tan, 2019: GPM IMERG Final Precipitation L3 Half Hourly 0.1 degree X 0.1 degree, Version 6. Goddard Earth Sciences Data and Information Services Center, accessed June 2022, https://10.5067/GPM/IMERG/3B-HH/06.

Miller, D. K., 2022: Great Smoky Mountain Rain Gauge Network Field Report. Great Smoky Mountain Rain Gauge Network Field Report 23 May 2022, 14 pp,https://www.atms.unca.edu/dmiller/GSMRGN_report_23may2022.pdf.

Miller, D. K., D. Hotz, J. Winton, and L. Stewart, 2018: Investigation of atmospheric rivers impacting the Pigeon River Basin of the southern Appalachian Mountains. *Wea. Forecasting*, **33**, 283–299.

Miller, D., J. Forsythe, S. Kusselson, W. Straka III, J. Yin, X. Zhan, and R. Ferraro, 2021a: A study of two impactful heavy rainfall events in the Southern Appalachian Mountains during early 2020, Part I; Societal impacts, synoptic overview, and historical context. *Remote Sensing,* **13**, 2452. https://doi.org/10.3390/rs13132452.

Miller, D., M. Arulraj, R. Ferraro, C. Grassotti, B. Kuligowski, S. Liu, V. Petkovic, S. Wu, and P. Xie, 2021b: A study of two impactful heavy rainfall events in the Southern Appalachian Mountains during early 2020, Part II; Regional overview, rainfall evolution, and satellite QPE utility. *Remote Sensing*, **13**, 2500. https://doi.org/10.3390/rs13132500.

Purdy, J.C., G.L. Austin, A.W. Seed, I.D. Cluckie, 2005: Radar evidence of orographic enhancement due to the seeder feeder mechanism. *Meteorol. Appl.*, **12**,

199–206, https://doi.org/10.1017/S1350482705001672.
Prat, O.P., and A.P. Barros, 2010a: Assessing satellite-based precipitation estimates in the southern Appalachian Mountains using rain gauges and TRMM PR. *Adv. Geosci.*, **25**, 143–153, https://doi.org/10.5194/adgeo-25-143-2010.
Prat, O.P., and A.P. Barros, 2010b: Ground observations to characterize the spatial gradients and vertical structure of orographic precipitation – Experiments in the inner region of the Great Smoky Mountains. *J. Hydrol.*, **391**, 141–156, https://doi.org/10.1016/j.jhydrol.2010.07.013.
Prat, O. P., and B. R. Nelson, 2015: Evaluation of precipitation estimates over CONUS derived from satellite, radar, and rain gauge data sets at daily to annual scales (2002–2012). *Hydrology and Earth System Sciences*, **19**, 2037-2056, https://doi.org/10.5194/hess-19-2037-2015.
Tao, Jing, and Ana P. Barros, 2013: Prospects for flash flood forecasting in mountainous regions – An investigation of Tropical Storm Fay in the Southern Appalachians. *Journal of Hydrology,* **506**, 69-89, https://doi.org/10.1016/j.jhydrol.2013.02.052.
U.S. Geological Survey, 2022: USGS 3D Elevation Program Digital Elevation Model, accessed June 2022, https://www.usgs.gov/3d-elevation-program.
Wilson, A. M., and A. P. Barros, 2014: An investigation of warm rainfall microphysics in the southern Appalachians: Orographic enhancement via low-level seeder–feeder interactions. *J. Atmos. Sci.*, **71**, 1783–1805, https://doi.org/10.1175/JAS-D-13-0228.1.
WMO, 2008: Precipitation gauge errors and corrections. Guide to Meteorological Instruments and Methods of Observation, 7th ed. WMO-8, I.6-6–I.6-7.

Appendix A

Gauge Number	Location	Latitude (N)	Longitude (W)	Elevation (m)
002	Lickstone Bald	35°25.5’	82°58.2’	1731
003	High Top	35°23.0’	82°54.9’	1609
004	Lickstone Ridge S	35°22.0’	82°59.4’	1922

005	Deep Gap	35°24.5’	82°57.8’	1520
008	Double Summer Gap	35°22.9’	82°58.4’	1737
010	Beaty Summer Gap	35°27.3’	82°56.8’	1478
011	near Deep Gap	35°23.7’	82°54.9’	1244
100	Purchase Knob	35°35.1’	83°04.3’	1495
101	The Swag	35°34.5’	83°05.2’	1520
102	Hemphill Bald	35°33.8’	83°06.2’	1635
103	JR Property	35°33.2’	83°07.0’	1688
104	Cat. Ski Area	35˚33.2’	83˚05.2’	1587
105	KH Property	35°38.0’	83°02.4’	1345
106	Pinnacle Ridge	35°25.9’	83°01.7’	1210
107	Lookout Point	35°34.0’	82°54.4’	1359
108	Utah Mountain	35°33.2’	82°59.3’	1277
109	Eaglesnest Ridge	35°29.7’	83°02.4’	1500
110	JH Property	35°32.8’	83°08.8’	1563
111	Hurricane Ridge	35°43.7’	82°56.8’	1394
112	Ore Knob	35°45.0’	82°57.8’	1184
300	Camel Hump Knob	35°43.5’	83°13.0’	1558

301	Mt Guyot	35°42.3’	83°15.3’	2003
302	Snake Den Ridge	35°43.2’	83°14.8’	1860
303	Mt Cammerer	35°45.7’	83°09.7’	1490
304	Big Cataloochee	35°40.2’	83°10.9’	1820
305	Mt Sterling 1	35°41.4’	83°07.9’	1630
306	Sunup Knob	35°44.7’	83°10.2’	1536
307	Balsam Mountain	35°39.0’	83°11.9’	1624
308	Cosby Knob	35°39.0’	83°10.9’	1471
309	Mt Sterling 2	35°40.9’	83°09.0’	1604
310	Mt Sterling 3	35°42.1’	83°07.3’	1756
311	Big Creek	35°45.9’	83°08.4’	1036

Table A1. List of rain-gauges in Duke GSMRGN used in this study.